https://doi.org/10.1016/j.ijheatmasstransfer.2018.12.147

Time-resolved droplet size and velocity distributions in a dilute region of a high-pressure pulsed diesel spray

Zehao Feng[1], Chenglong Tang[1]*, Yue Yin[2], Peng Zhang[2]*, Zuohua Huang[1]

[1]State Key Laboratory of Multiphase Flow in Power Engineering,

Xi'an Jiaotong University, Xi'an, 710049, People's Republic of China

[2]Department of Mechanical Engineering, The Hong Kong Polytechnic University, Hung Hom, Hong Kong

Abstract

The principal objective of the present work is to experimentally investigate the time-resolved spray characteristics. Droplets data in a dilute region of a high-pressure diesel spray were obtained by employing the PDIA (particle/droplet image analysis) method with double pulse laser illumination. Eulerian specification was adopted to describe the transient spray microscopic behavior within a fixed test window at ten representative instants after triggering the injection. The experimental results indicate that the transient spray evolution can be characterized in three distinct stages. During stage I (the latency stage), the spray tip develops and reaches the test location, but no discrete droplets were clearly observed. During stage II, the spray passes through the test window, from which discrete droplets are observed to disperse in the dilute region and the SMD of the droplets increases rapidly. During stage III, bulk spray disappears in the test window and only discrete droplets were observed. The SMD of the droplets is decreased to a "steady-state" value. Based on these sampled and processed data, the droplet size distribution functions were obtained and compared with the Rosin-Rammler and the Nukiyama-Tanasawa function. Finally, the Stokes number and the Weber number of each droplet were determined, and the movement of the droplets were analyzed. The measured time dependent droplet behaviors are believed to provide important data for spray modeling and simulation.

Key words： diesel spray; droplet size and velocity distribution; distribution functions; SMD.

* Corresponding authors:

chenglongtang@xjtu.edu.cn (C. Tang)

pengzhang.zhang@polyu.edu.hk (P. Zhang)

1. Introduction

Understanding and therefore controlling diesel sprays is essential for improving engine performance and meeting increasingly stringent emission regulations[1, 2]. Research works related to the "macroscopic characteristics" of diesel sprays, for example the spray penetration, the spray cone angle, and the spray projected area, have been extensively conducted [3-6]. However, the "microscopic characteristics" of diesel spray, for example the droplet size, the velocity and number density distributions, are important properties that will affect the local equivalence ratio and required to be accurately predicted by spray modeling in computational fluid dynamics (CFD) [2].

Accurate description of the drop size distribution as a function of the system thermodynamic conditions is essentially important for analysis of the phase phase change, heat and mass transport in all kind of dispersed systems. For example, the droplet size distribution in an engine is important to study the frequency of coalescence, rate of evaporation, amount of entrainment and burning of droplets. Theoretically, all sorts of microscopic characteristics can be derived from the droplet distribution function, which determines the probability of finding a droplet of certain radius and velocity at a given time and location. For mathematical convenience, it is useful to introduce the concept of differential probability $f(r,\boldsymbol{x},\boldsymbol{v},t)\mathrm{d}r\mathrm{d}\boldsymbol{x}\mathrm{d}\boldsymbol{v}$, which is the probability of finding droplets in the radius range (***r*** **,** ***r***+d***r*****),** in the velocity range (***v*** , ***v*** +d***v*****),** in the spatial range (***x*** , ***x*** +d***x*****)** and at the time *t.* The transport equation of the distribution function f is analogous to that of the kinetic theory of gases,

$$\frac{\partial f}{\partial t} = -\frac{\partial}{\partial r}(Rf) - \frac{\partial}{\partial \boldsymbol{x}}(\boldsymbol{v}f) - \frac{\partial}{\partial \boldsymbol{v}}(\boldsymbol{F}f) + Q + \Gamma\,, \tag{1}$$

where the rate of change of the droplet size is $R = (\mathrm{d}D/\mathrm{d}t)$, and the force per unit mass is $\boldsymbol{F} = (\mathrm{d}\boldsymbol{v}/\mathrm{d}t)$. The first source term Q denotes the rate of change of f with time induced by droplet formation or destruction, and the second source term Γ represents the rate of change of f caused by collisions with other droplets.

It is practically difficult to collect all the information of every droplet to construct the distribution function of eight dimensions and solve the full spray

equation. Consequently, they are often reduced to applicable and solvable forms. Of these reduced forms, the most encountered in practice is the presumed size distribution $f(r,\boldsymbol{x})$ at position $\boldsymbol{x}$ in a steady-state flow field. The general Rosin-Rammler function [7] and Nukiyama and Tanasawa [8] function

$$\mathrm{f} = \mathrm{b}\mathrm{d}^{\mathrm{m}}\exp\left(-ad^{n}\right)$$

$$\mathrm{f} = k_d\mathrm{d}^{p}\exp\left(-cd^{s}\right) \qquad (2),$$

have been widely employed in application[9]. Because of crucial role of the distribution function in describing the droplet microscopic characteristics, one of the most important objective of a spray study is through experiment to collect adequate data to construct the reasonable distribution functions. Through these processed data and functions to analyze the corresponding properties, behaviors of spray/droplets.

Owing to the development of the high-speed imaging and laser diagnostic technology, several attempts to investigate the droplet microscopic behavior have been conducted [2, 10]. For steady atomization process with a constant liquid fuel flow that typically happens in gas turbines and aero engines, the droplet spatial distribution at both low- and high-temperature conditions have been studied. Specifically, Urban et al. [11] studied the spray microscopic characteristics by using a plain-jet air-blast atomizer with a fixed flow rate and the phase-Doppler technique. Their results show that droplet radial velocities increase significantly with the injection pressure. In addition, the most intense atomization locates in the central region, and the droplets at the periphery are highly stable. Kulkarni and Deshmukh [12] experimentally measured the SMD (Sauter Mean Diameter) and the droplet size distribution at different points in an air-blast atomizer spray. Their results show that the SMD at the periphery is higher than that along the axis of the spray because of the swirling atomizing air from the nozzle.

For a pulsed injection transient spray, which is typically used in gasoline or diesel engines, more works have been conducted to achieve a complete mapping of the dependence of droplet size and velocity on spatial location within the spray. Lee

and Nishida [13] used a microscopic laser induced fluorescence (LIF) imaging technique to obtain the high spatial resolution LIF tomograms of the pre-swirl spray. They found that the SMD of the pre-swirl spray during the breakup of the liquid blob is very large with a large scattering, and then it steeply decreases during the breakup processes of the long-ligaments and the small-sized liquid blobs. They also found that the small-sized droplets show a very broad axial and radial velocity range, while the large-sized droplets show a relatively narrow velocity range similar to the mean velocity of the whole of the pre-swirl spray. Komada et al. [14] used a laser 2-focus (L2F) velocimetry technique to measure the velocity and size of droplets at the injection pressure of 800 bar in diesel sprays. They observed that droplets at the center have a higher velocity and the velocity decreases from the center towards the spray periphery. Li et al. [15] investigated the spray of a multi-hole DI injector by using a PDPA (Phase Doppler Particle Analyzer) technique over a range of ambient and injection pressures in a constant volume vessel. They measured the SMD at different radial positions at different ambient pressures and found that SMD increases at elevated ambient pressures. For a fixed ambient pressure, SMD also increases as the measurement position moves towards the outer edge of the spray. It is noted that their measured droplet size distribution is based on an average of a 1.5 ms pulsed spray. Payri and co-workers performed phase Doppler anemometry measurements to obtain the local droplet velocity [10]. They found that the average droplet velocity decreases along with the axial direction down the nozzle, and that the droplet velocity at a given axial position decreases as the measurement point shifts to the outer periphery of the spray. Payri et al. [2] provided the velocity field of the diesel spray by applying the PIV (Particle Image Velocimetry) technique with droplets as the seeding particle, but the measurements were limited to the steady stage of a fully developed spray. Jedelsky et al. [16] calculated the droplets Stokes Numbers were at different regions in pressure-swirl atomizer sprays. They showed that droplets < 5 μm followed the airflow faithfully and so can be used to estimate the local airflow velocity. In addition, they found that their Stokes number reduces with the axial distance and increases with droplet size.

Recently, the image-based droplet sizing techniques have drawn increasing attention [17, 18]. Particle/droplet image analysis (PDIA) is an imaging approach for flow field characterization. By using the laser pulse with a width much shorter than the time scale of the transient spray process, the image of the droplets within the target window can be directly captured with the long focal-length microscope. Kashdan et al. [18] has compared the PDIA and PDA approaches for droplet sizing determination, and they showed that for the droplets in the size range between 5 and 30 μm, the results by these methods are very consistent. They also indicated that the PDIA technique has the advantage of being able to determine non-spherical large size droplets, while the PDA technique presumes spherical droplets, which may not be valid for larger droplets.

The above literatures focused on the spatial distribution of the droplet size and velocity within the spray. For a stationary atomizer spray such as that in [12], the spatial distribution of the spray microscopic parameters such as the SMD and velocity can be resolved with the laser diagnostic techniques. For a pulsed spray that is typically used in reciprocating piston diesel or gasoline engines, however, most of the previous works consider only the steady state of a fully developed spray or use ensemble average to obtain the spray microscopic statistics. A direct injection of a pulsed spray consists of sub-stages of the nozzle valve opening, holding and closing which happens in a time scale of several milliseconds. As such the spray microscopic characteristics are expected to be strongly time dependent, while the time resolved microscopic behaviors such as the droplet size and velocity distribution have not been reported previously. Evidently, these data are valuable for spray model validations.

Only a few studies have been attempted on the time-dependent characteristics of pulsed sprays. Keller et al.[19] investigated the local droplet size distribution of pure iso-octane and ethanol sprays under gasoline engine conditions by using a PDPA technique, although only two-time instants were studied. They found that, for the iso-octane spray, the droplet size distribution at fixed operating point can be described by the Rosin-Rammler distribution at the two instants after the injection. However, for the ethanol spray, droplet size distributions at two instants are different because

smaller droplets disappear earlier due to the fast evaporation nature of ethanol. Jing et al. [20] recently also measured the time-averaged SMD and velocity as a function of the spatial location within the sprays of diesel, gasoline and their mixtures by using a PDPA technique. They showed that both the SMD and the velocity decrease along the axial distance from the nozzle. Recently, Pathania et al. [21] studied the droplet size statistics of a single hole spray from pulsed port fuel injector along the spray penetration axis by using a PDPA technique. The average droplet diameter is of the order of 100 μm and increases along the axial distance below the nozzle tip. For large size droplets reported in their work, the measured instantaneous droplet diameter shows a significantly large pulse to pulse variation, possibly due to the non-sphericity of droplets. In addition, they also showed that the average droplet size does not vary significantly with time after the start of injection.

Since most of the previous studies on microscopic droplet size statistics consider only the steady, fully developed spray, the present paper features the following three aspects. First, we use our PDIA system to resolve the time dependence of the droplet size statistics observed in a fixed test window within a high-pressure diesel spray by accurately controlling the laser pulse trigger after triggering the injection. It should be noted that the PDIA system [22, 23] cannot resolve the dense spray region, so it focuses on a dilute spray region, where the density of liquid phase is appropriate for accurate droplet recognition. In addition, experimental measurements are then used to validate two widely used distribution functions including that of Rosin-Rammler and the Nukiyama-Tanasawa, for all time instants. Second, considering that most of previous experimental works on pulsed sprays reported the droplet velocity during the quasi-steady evolution stage of spray when the needle valve is fully open, we tuned the delay time of the double pulsed laser so as to resolve the droplet velocity during the whole spray stage. Furthermore, the interaction between the droplets and the initially quiescent gas induces local gas flow and causes droplet breakup, which are also time dependent. Several previous work intended to understand the droplet-gas interaction by use of the Stokes number (quantifying the tendency of droplets being tracing particles) and Weber number (quantifying the tendency of droplet breakup)

[24-28], but none of them targeted on pulsed sprays. Hence the third objective of the present study is to present statistics on the time resolved droplet Stokes number and Weber number in order to enhance the understanding of the droplet-gas interactions, which will be useful for modeling the source term Q in Equation (1).

For expatiating the stated objectives and features, the paper is arranged in four sections. In Section 2, the experimental setup will be specified, followed by the discussion about the measured droplet size and velocity that characterize the spray microscopic behaviors. In Section 3, droplet distribution functions are built based on the sampled data and the evolution of the transient spray is analyzed by employing these processed data. In Section 4, the conclusions are drawn and future works are proposed.

2. Experimental setup

2.1. Experimental system

Experimental test rig has been described in detail in our previous works [22, 23]. Briefly, the system consists of a constant volume chamber with optical access, high pressure fuel supply assembly with water cooling, and the synchronization circuit. High pressure common-rail injection system and the injector with a single nozzle hole is used to generate high pressure diesel spray. The rail pressure and the injection duration are monitored, and the double pulsed laser delay, the camera, and the injector trigger signals are synchronized by the ECU (optical diagnostic controller OD2301). The PDIA system is applied as the optical diagnostic technique and the detailed introduction will be present in Sec. 2.2.

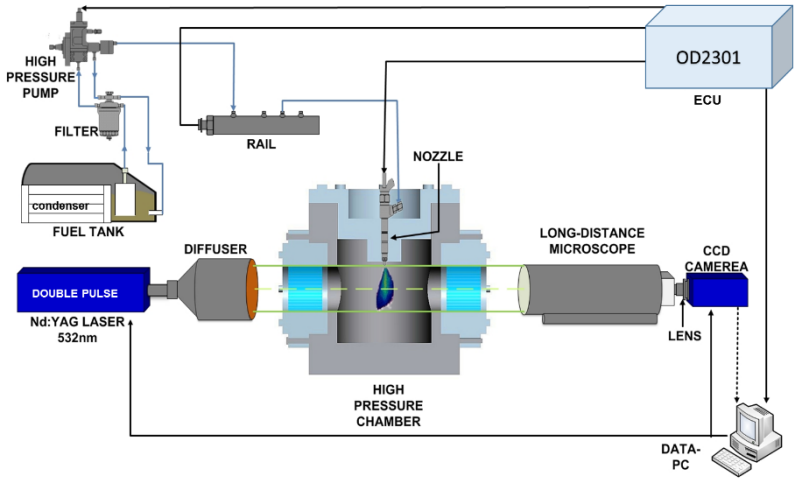

Figure 1. Schematic diagram of experimental apparatus.

2.2. PDIA system

The PDIA is a shadow-graphic approach that only captures the isolated liquid droplets on the focal plane. A double pulsed Nd:YAG laser with the wavelength of 532 nm is employed as the light source and the measured intensity of each laser beam is 220 mJ/pulse. The duration of the two pulses is 5 ns, which is much shorter than the injection duration and the spray evolution so that the time counting can be of good accuracy and the corresponding image is of high resolution. A diffusor with a dye plate is attached to the laser for uniform backlighting. The diameter of the lens at the head of the diffusor is 120 mm which is larger than the diameter of the chamber window, so that the whole field of view is uniformly illuminated. A CCD camera (ImagerProSX 5M, 2456 × 2058 pixels), attached with a long-distance microscope (LDM, Queststar QM1) and a 2X Barlow lens are used to capture the local droplets. The LDM has a working distance of 0.56 – 1.52 m with a minimum field of view of 1.2 mm x 1.2 mm. The camera and the LDM are mounted on an electrically controlled three way-positioner MC600 with a displacement accuracy of 1 μm to ensure the accurate determination of the scanning target location.

To determine the size and velocity of individual droplets, the laser and the camera are operated in the double-pulse, double-frame mode. Fig. 2 shows part of the

two typical images obtained by flashing two laser pulses with a delay time of Δt for one injection event. The two-frame image is processed by the software DaVis 8.4 of LaVision. In the procedure, an appropriate threshold value (30%) is applied to the image in order to distinguish the droplets from the illumination background. Then the image will be scanned by the automated algorithm pixel by pixel. A pixel is identified as an element of a certain segment when its intensity is above this threshold value so that each segment consists of contiguous pixel areas. Regions of the image which have an intensity less than the global threshold are ignored. Then, a high and low level (35% and 65%) as percentage of the minimum and maximum intensities of each segment are defined. The algorithm will also count the number of pixels above both the high level and the low level. Eventually the center of mass, the particle diameter and the eccentricity are calculated by averaging the two values.

The droplet velocity is determined by counting its displacement Δs in the two frames during the delay time Δt of the two laser pulses. To identify the displacement of the same droplet in the two frames, two parameters of the algorithm are selected to ensure the accuracy of recognition unit: one is the limited size variation (15% difference) and the other is the allowed shift (up to 50 μm).

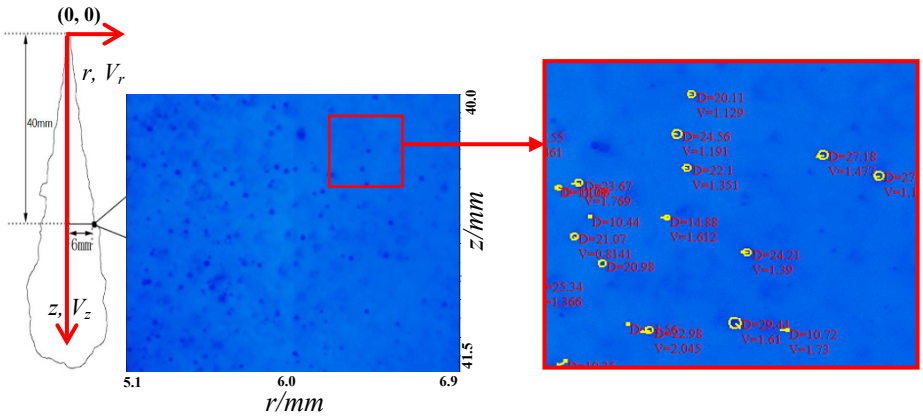

Figure 2: Measurement location for microscopic behaviors and typical double-frame image obtained by PDIA.

The uncertainty in the droplet size determination primarily comes from the depth of field which is third direction limiting the probe volume [29]. With increasing

distance from the focal plane, the contour of the particles becomes increasingly blurred with smoother intensity gradients and reduced shadowing effect. A larger droplet has a higher probability to get identified as compared to a small droplet. As a result, the captured images show a bias towards larger droplets. Therefore, the detection probability has been calibrated to increase the relative weighting for the small particles in order to correct this effect. Furthermore, the present PDIA technique for droplet size determination is calibrated by the standard isolated particles with known size and the maximum error is found to be less than 2%.

2.3. Experimental procedure

Commercial diesel (density, viscosity and surface tension of commercial diesel are measured to be 83.7 kg/m^3, 2.96 mPa.s and 25.9 mN.m respectively) is used. The injection pressure and ambient pressure is 1000 and 20 bar respectively with the temperature fixed at 25 ^{0}C. We fixed the measurement window at the location of Z = 40 mm below the nozzle tip and R = 6 mm off the spray axis as shown in Fig.2. After scaling with a scaling plate (minimum scale of 25 μm and total length of 5 mm), the size of the window is 1.8 × 1.5 mm^2 which gives a resolution of 1.37 μm/pixel. The minimum droplet size detectable with good accuracy for the technique corresponds to 5 times the pixel size ($\approx$ 6.85 μm).

Fig.3 shows pulse sequence of different trigger signals in this investigation. By synchronizing of the laser pulse trigger signal and the injection trigger signal through the ECU, the droplet image at different delay time can be captured by the long focus microscope and CCD camera. Time zero (t = 0) is determined when the spay just exits from the nozzle (STP = 0), as shown in Fig. 3. Then the laser pulse trigger is gradually tuned to realize snapshot at different time instants in the range between 0 and 13 ms. In order to obtain statistically reliable data, at least 100 images and no less than 6000 droplets were counted for each experiment such that the statistical droplet SMD is independent of the number of droplets.

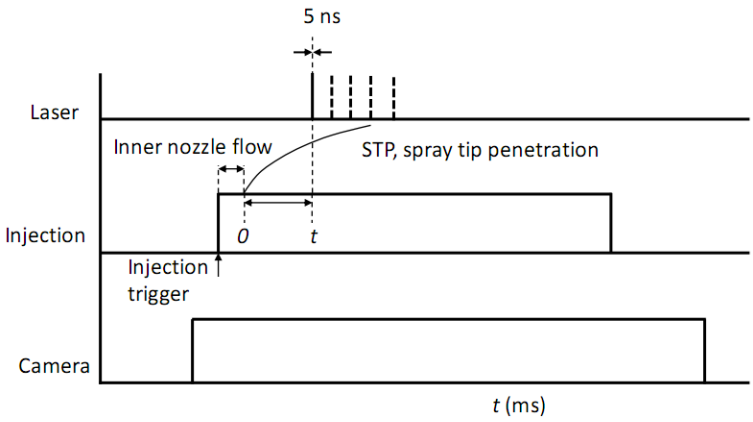

Figure 3: The pulse sequence of the signals of injector, laser and camera.

3. Results and discussion

3.1. Spray macroscopic and microscopic evolution

Figure 4(a) shows the macroscopic evolution of the spray captured using high speed photography and scattering light illumination. The red square represents the fixed test window to investigate microscopic behavior characterization for the Eulerian specification of the flow field. The recorded images are then converted into pseudo color images according to local pixel gray value. This value indicates the intensity of the scattering light, which also indicates the liquid phase density [30]. These macroscopic images demonstrate the different stages of the spray evolution and the relative location of the macroscopic spray body with respect to the fixed test window. It indicates that the earliest instant that the spray tip reaches the test window is at time t = 0.5 ms. The period before t < 0.5 ms is defined as stage I, in which the tip of spray just has not yet reached the test window, and no individual droplets are found. After that, the spray keeps on evolving and passes across the test window. At t = 2.1 ms, the fuel injection is finished, and no more liquid momentum is further depositing into the spray. The period 0.5 ms< t $\leqslant$ 2.1 ms is then defined as stage II, in which there is a continuous liquid transport from the injection nozzle. After 2.1 ms, the spray develops freely, and it is recognized as stage III. We note that the region with low liquid-phase density firstly locates around the waist of the spray and accounts for only a small fraction of the total spray area, as shown by the images for t $\leqslant$ 0.5 ms. Subsequently,

more and more low liquid-phase density region is formed at the tip of the spray, as shown by the images for 0.5ms < t < 2.1 ms. After t = 2.1 ms, the high liquid phase density region breaks into isolated agglomerations and gradually vanishes. The gray value qualitatively indicates the liquid-phase density, and the calculated mean gray value of the test window is shown in Figure 4(b). Before t=0.5 ms, the mean gray value of the test window is zero, then it increases as the liquid phase passes across the test window. It peaks at around 2.1 ms and gradually declines as time evolves.

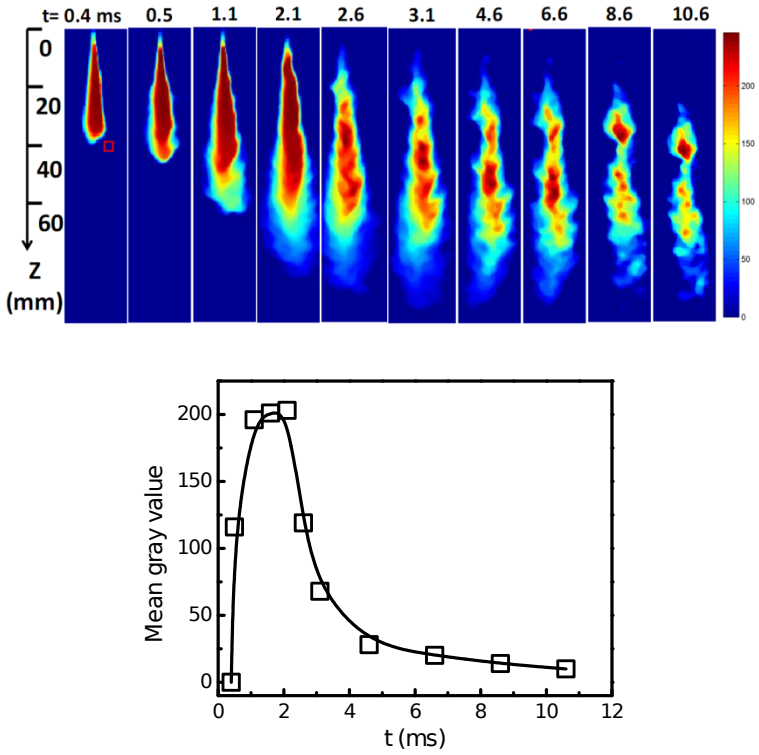

Figure 4: (a) The evolution of a pulsed spray (b) the mean gray value of the test window indicated by a red square.

Typical droplet images obtained by the PDIA system at different times are presented in Figure 5. No droplets were observed before t=0.5 ms, because the spray tip just enters the target field of view and the observed spray tip receives fast momentum transfer from the upstream resides in the dense region. As time evolves, the tip and then the periphery region of spray body passes over the window. At t = 0.6 ms, isolated droplets were observed in the test window and only half of the window are filled with droplets. In the following 1.5 ms (0.5 ms< t < 2.1 ms),

increasing amount of liquids were observed. After t = 2.1 ms, the spray injection is finished. The spray evolves and penetrates by its own inertia and air drag, and there is no momentum transform from the nozzle exit. It is observed that many droplet clouds are disappeared and the whole window is covered with isolated and dispersed droplets and as time evolves, the droplets are even more dilutely distributed. After t > 10.6 ms, the counted number of droplets becomes too small for a physically meaningful statistics. As such, ten sampling time instances from 0.6 ms to 10.6 ms are processed, and they constitute valid statistical analysis in the following.

Primary atomization occurs at or near the nozzle exit where bulk fluid, typically in the form of sheet or jet, breaks up for the first time and forms the ligaments and droplets. The ligament formation is strongly correlated with the sheer stress caused by high-speed liquid injection. This is followed by secondary atomization, which typically occurs further downstream and is also strongly affected by the sheer stress. At the spray periphery near the spray tip, the initial droplets or ligaments after primary breakup have relatively high velocities. Strong aerodynamic forces cause the droplets to deform and break apart into smaller ones, as observed by the increasing amount of droplets during Stage II (0.6~2.1 ms). As the spray develops for around 2.1 ms, the liquid momentum transported from the injection nozzle reduces because of the close of the needle valve, the droplets in the test window just diffuse apart, as observed by the images at t=2.6~12.6 in which droplets becomes progressively dispersed.

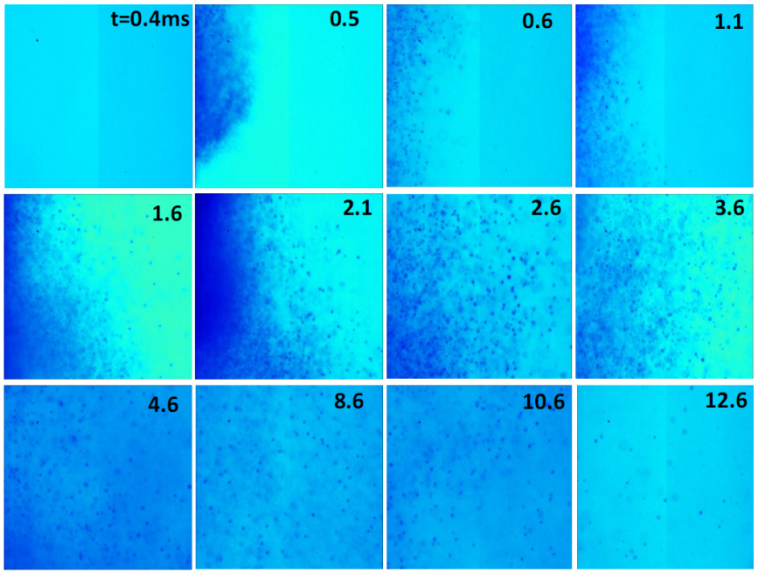

Figure 5: Typical original microscopic droplet images at different times from the PDIA system.

3.2. Time-resolved droplet size statistics

As discussed previously, when t < 0.6 ms, the spray development resides in the first stage and the spray tip just arrives at the test window and there are no sufficient droplets for statistics. Figure 6 shows the measured size PDFs of droplets after t=0.6ms. It is seen that the diameters of droplets are in the range of 7.0- 46.5 μm. During 0.6 ms < t < 2.1 ms, the peak value (the maximum probability density) of the PDF decreases from 0.12 to 0.08 and shifts to larger droplet size. This may imply frequent droplet collision and coalescence during the developing stage. The measured size PDFs for stage III (2.1 ms < t < 10.6 ms) are all collapsed, as shown in Figure 6(b), and imply the droplet size distribution reaches an "equilibrium state". Physically, we can infer from this result that droplet breakup and coalescence become insignificant as the droplets in the spray becomes progressively dilutely dispersed with time.

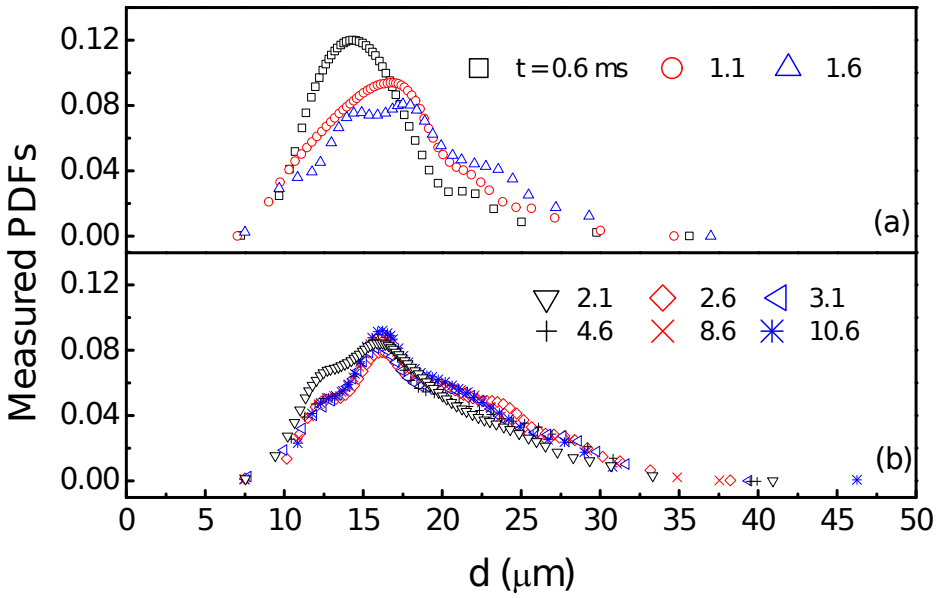

Figure 6: Measured PDFs of droplet size in (a) stage II and (b) stage III.

The further analysis on the microscopic characteristics of spray is carried out by fitting the CDF (Cumulative Distribution Function) of droplet diameter. B-spline curve in conjunction with the least square method is utilized to fitting the CDF from the experimental data. The CDF, mostly like a sigmoid curve, can be expressed with B-Spline function as

$$\mathrm{CDF(x)} = \sum_{j-k+1}^{j} c_{i,k} B_{i,k}(x) \tag{3},$$

wherein the $B_{i,k}$ is the basis function, $c_{i,k}$ is the control point (de Boor point). With stable algorithm by Carl de Boor, the k-order, (k-1)-degree of B-Spline basis function recursively is calculated by

$$B_{i,k} = \frac{x - t_i}{t_{i+k-1} - t_i} B_{i,k-1}(x) + \frac{t_{i+1} - x}{t_{i+k} - t_{i+1}} B_{i+1,k-1}(x) \tag{4}$$

The PDF (Probability Density Function) of droplet size is determined by the first derivative of the CDF

$$PDF(x) = \frac{\mathrm{d}\, CDF(x)}{\mathrm{d}\, x} = \sum_{j-k+1}^{j} c_{i,k} \dot{B}_{i,k}(x) \tag{5}$$

To obtain physically meaningful PDF, we fitted the measured PDF by using the log-normal, the Nukiyama-Tanasawa and the Rosin-Rammler distribution functions, and the comparison result is shown in Figure 7. Although none of these distribution

functions can exactly reproduce the hut-form part around mean value μ (nearly [μ-2.5, μ+2.5] μm), it is interesting to find that the time-dependent PDFs of experiment can be well approximated by the lognormal distribution function

$$f(d) = \frac{A}{\sqrt{2\pi}d\sigma} * exp\left(-\frac{(ln\, d - ln\, \mu)^2}{2\sigma^2} \right) \quad (6)$$

where μ is the mean diameter, A is the amplitude, and σ is the standard variance as shown in the inset of Figure. 7(d). The amplitude of the lognormal function changes slightly between 1.0 to 1.065, and the standard variance also has a sight change between 0.27 and 0.33, as shown in the embedded subfigure in Figure 7(d). This result means that the lognormal fitting by Eq. (6) well captures the time-dependence of the measured PDFs. Further comparison between the distribution functions for deciding their superior over the others seems to be of less importance because they are all fitting formulas in nature. Our preference to the lognormal distribution is mainly owing to its simplicity in both mathematical form and physical meaning, and to its performance in fitting the time-dependent PDFs. Future works on this issue is certainly merited.

The statistic Sauter Mean Diameter (SMD) is presented in Figure 8. It is worth mentioning that the PDIA system only counts the dispersed droplets in the dilute region and does not recognize the dense region in the spray center where the droplet number is too dense. As a result, only individual droplets that are captured in the test window per injection are counted. It is observed that the SMD is initially small (17.64 μm) and gradually increases to a maximum value of around (23 μm) at about 2.6 ms and then-decreases to a nearly constant value. We note that the weak decrease of the SMD is not caused by droplet breakup because at this stage there is no more momentum depositing into the spray from the injection nozzle and the shear stress of the liquid phase is expected to decrease. Instead, our previous studies [22, 23] on the droplet size spatial distribution shows that there is a weak increase the SMD along with the radial direction from the inner to the spray periphery region. Because as the spray develops freely, the droplets become more dilute and the test window moves relatively from the periphery region to the inner region where the droplet size is

slightly smaller.

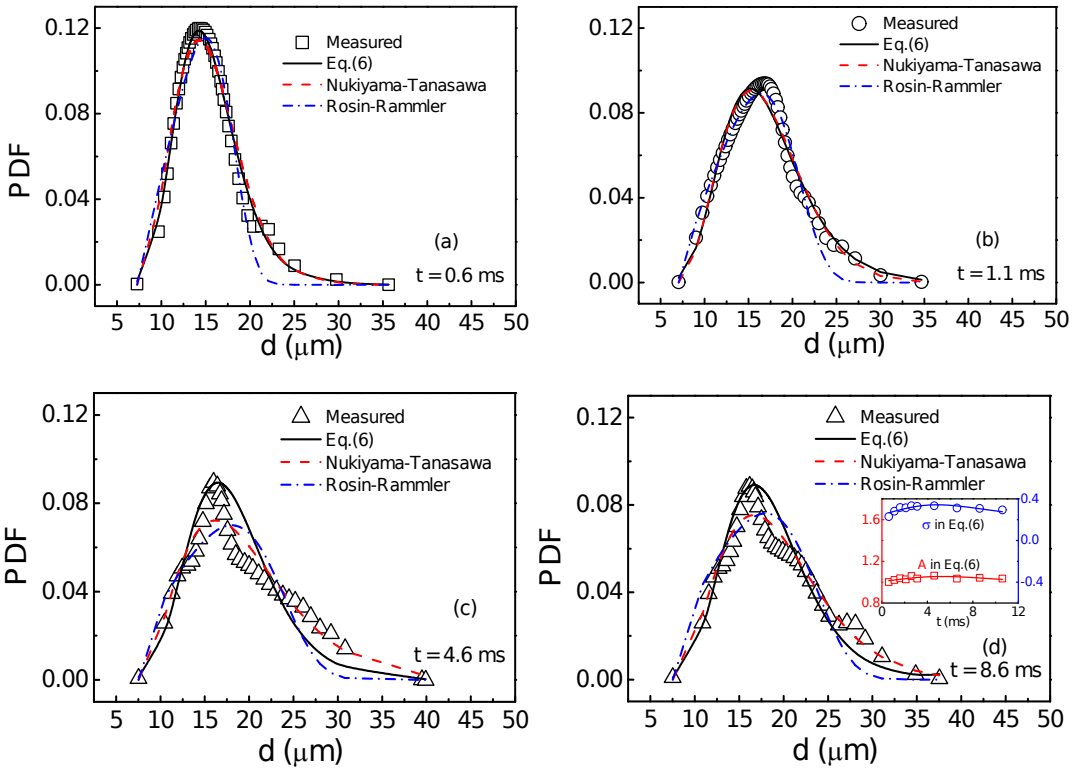

Figure 7: Comparison between the measured PDF of droplet size with different fitting functions.

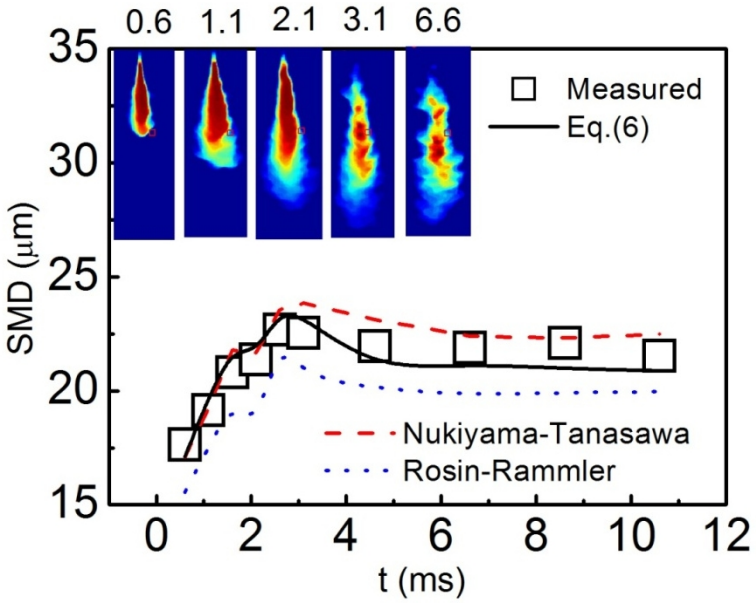

Figure 8: Variation of SMD as a function of time.

3.3. Time-resolved droplet velocity statistics

The PDF in velocity space reflects the dynamic properties of droplets. The mass-averaged velocity is calculated by

$$V = \frac{\sum d_i^3 V_i}{\sum d_i^3} \tag{7}$$

where d_i and V_i are the diameter and velocity (components or magnitude) of the i^{th} droplet. The mass-averaged velocity component r, z directions and the magnitude are presented in Figure 9.

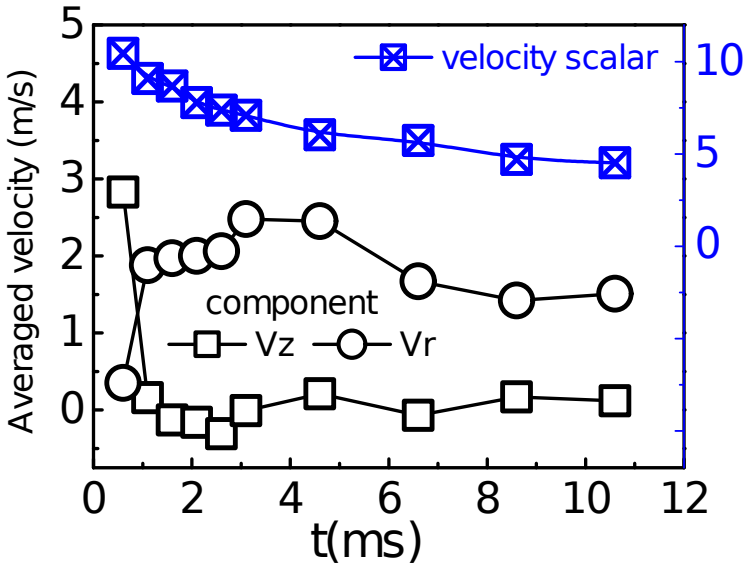

Figure 9: Mass-averaged droplet velocity component and magnitude as a function of time

The z-component of velocity shows that the spray flows through the window with a relative large velocity (about 3.0 m/s) at the beginning. Because of the interaction of droplets with the ambient air, this velocity component tends to zero at the end of pulse. The r-component is initially small and it increases to a maximum value of around 2.5 m/s at around t = 3.1ms. This behavior reflects the entrainment under the action of air. The initial droplets have relatively large downward momentum and later the kinetic energy of the liquid droplet continuously decreases due to the drag resistance [20].

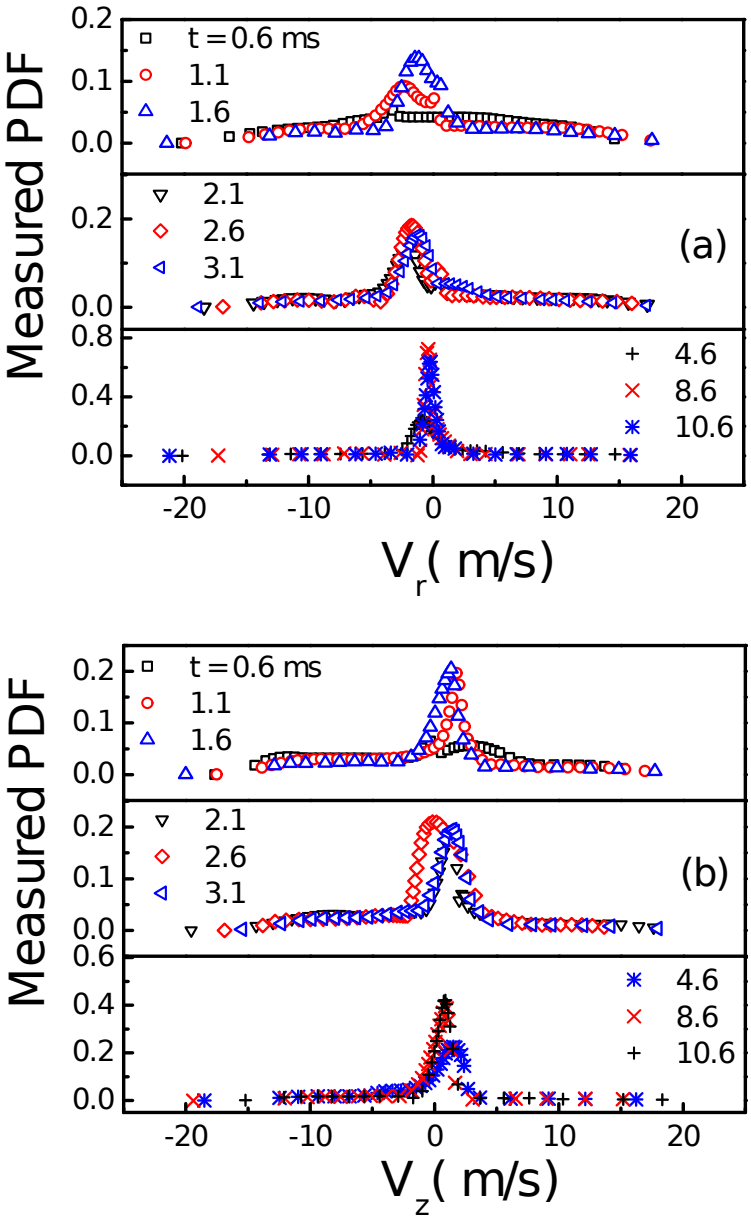

Figure 10: Measured PDFs of droplet relative velocity for (a) the radial component and (b) the axial component.

With removing the effect of mass-averaged velocity, the measured PDFs for relative velocity are shown in Figure 10. The maximum value of the PDF at t=0.6ms is nearly 0.07, but both of z and r directions have a wider spectrum. It reflects at the beginning most droplets have non-zero velocity obviously. From t=1.1ms to 2.1ms, the peak value of the PDF of V_r is nearly 0.22. The increase of the peak value is because the initial momentum is consumed in the direction and more droplets tend to slow down. It is interesting to find that the relative velocity V_z corresponding to the

peak value of its PDF is negative but is positive for V_r. This is because V_z of most droplets is smaller than their mean velocity, and the droplets will hence "squeeze" each other to consume their momentum by interaction.

3.4. Droplet Stokes number

For the spray experiment, it is often questioned whether and to what extent the droplet velocity distribution provides information about the local gas flow. To answer the question, the Stokes number (*Stk*) of each droplet is calculated by Eq. 8 as in Ref. [Jebakumar A S, Abraham J. Comparison of the structure of computed and measured particle-laden jets for a wide range of Stokes numbers[24]

$$Stk = \frac{\tau p}{\tau f} \ , \tau_p = \frac{\rho_f d^2}{18\mu_g} \ , \tau_f = \frac{d}{v} \tag{8}$$

where τ_p is the particle response time, τ_f is the flow response time, ρ_f is the fuel density, d is the droplet diameter, μ_g is the viscosity of the ambient gas, and v is the droplet velocity. For those droplets with $Stk >> 1$, their trajectories are less affected by local gas flow [24, 25]. It should be noted that the velocity component in the direction normal to the test window cannot be measured in the present experimental apparatus, and that it is expected to be substantially smaller than the other two velocity component because the spray has no initial circumferential velocity. As a result, the Stokes number defined by Eq. (8) can be treated as a low bound of the actual value of droplet stokes number. It will be seen that considering slightly larger values of actual Stokes number substantiates the conclusions to be made shortly below.

The Stokes number of each droplet at t = 0.6 ms and t = 2.1 ms are presented in Figure 11, where different colors of the scatters indicate the range of *Stk*. The droplets of large *Stk* would take a longer time to adjust to the flow and the flow will have a less influence on the droplet trajectories. At t=0.6 ms, most *Stk* are larger than 100. This indicates that the droplet velocity cannot represent the gas velocity that is induced by momentum exchange from the droplets. At t=2.1 ms, most of the droplets still have large *Stk*, although they have a wider range of diameters.

To further examine the extent of interactions between the droplets and the ambient gas, we counted the number of droplets of different range of Stokes numbers as a function of time, as shown in Figure. 12. It is seen that initially the probability of the droplets with *Stk*>100, denoted by $P(Stk > 100)$, is the larger than those of the other three ranges $Stk < 1$, $1 < Stk < 10$, $10 < Stk < 100$. $P(Stk > 100)$ decreases and $P(1 < Stk < 100)$increases gradually with time. This indicates that most of the droplet trajectories are influenced by droplet breakup and collision, but not by the interaction with the gas phase.

It is seen that at around t=2.1 ms, there is a slight perturbation in $P(Stk > 100)$ and $P(1 < Stk < 100)$. This is because the spray development transits from stage II to stage III at the time, and the liquid momentum transport from the injection nozzle stops because of the close of the needle valve. As a consequence, the droplets in the test window receive a reduced momentum transfer from the upstream droplets and there is an increase of the diameter and decrease of the velocity in vertical direction as respectively seen in Figure 7 and Figure 11. As such, the number of droplets with *Stk* larger than 100 shows a perturbation at around t=2.1 ms.

Furthermore, there are trace amounts of droplets with *Stk* < 1 during the whole spray development process. These droplets, which have extremely small velocity, would adjust quickly to any changes in the flow and the local fluid streamlines cause curvature in particle trajectories[24, 25]. This indicates that the local gas flow has a very low velocity. This inference is reasonable because the initial gas is quiescent, and the only cause for the gas flow is the momentum exchange between the liquid droplets and their surrounding gas.

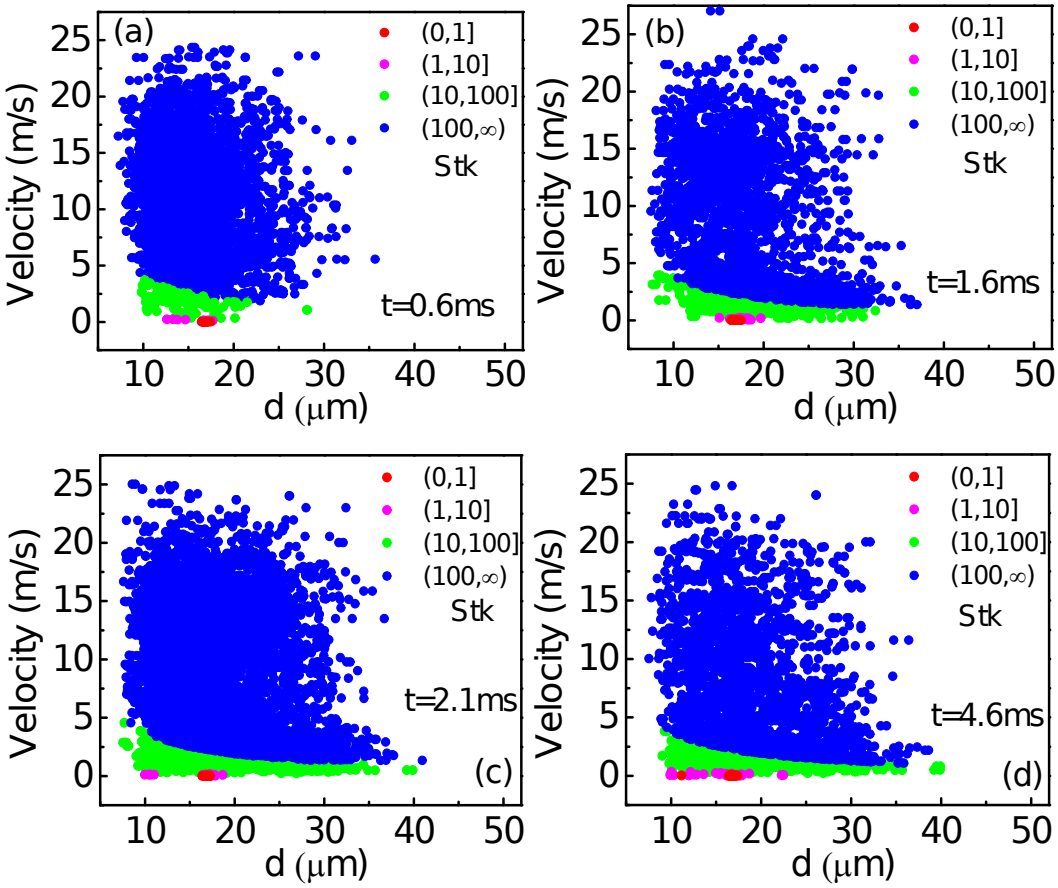

Figure 11. Range of *Stk* of all droplets during Stage II (t = 0.6 and 1.6 ms) and Stage III (t =2.1 and 4.6 ms)

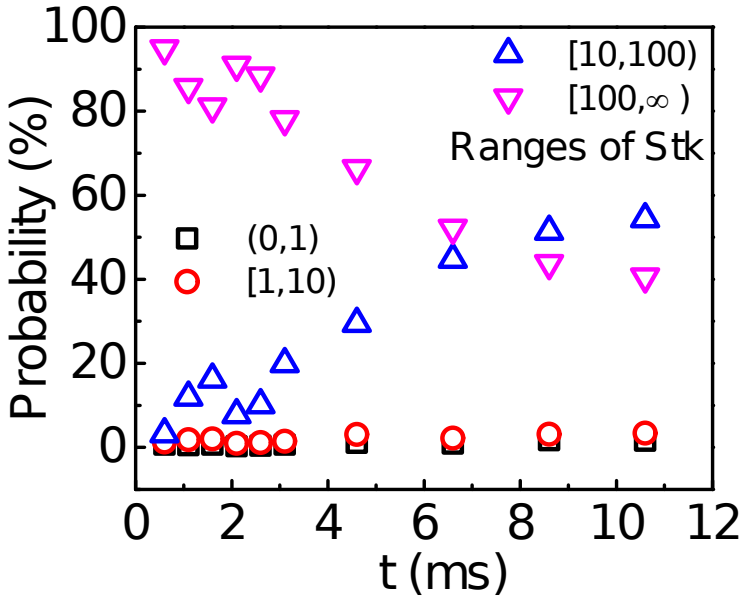

Figure 12 Variation of probabilities of droplet Stokes numbers with time.

3.5. Droplet Weber number

The droplet Weber number, *We*, defined as the ratio of the disrupting aerodynamic forces to the restorative surface tension forces, is the most important parameter describing secondary atomization of droplets, as a larger *We* indicates a higher tendency toward fragmentation [23, 31]. To represent the breakup behavior, the present Weber number is defined by

$$We=\rho_g u^2 d_0/\sigma \tag{9}$$

where ρ_g denotes the gas density, u is the relative flow velocity, d_0 is the initial droplet diameter, and σ is the surface tension coefficient. It will be seen shortly that the majority of the droplets have significantly higher velocity than the gas flow so that we can use the droplet velocity to approximate the relative velocity of the droplet with respect to the gas flow.

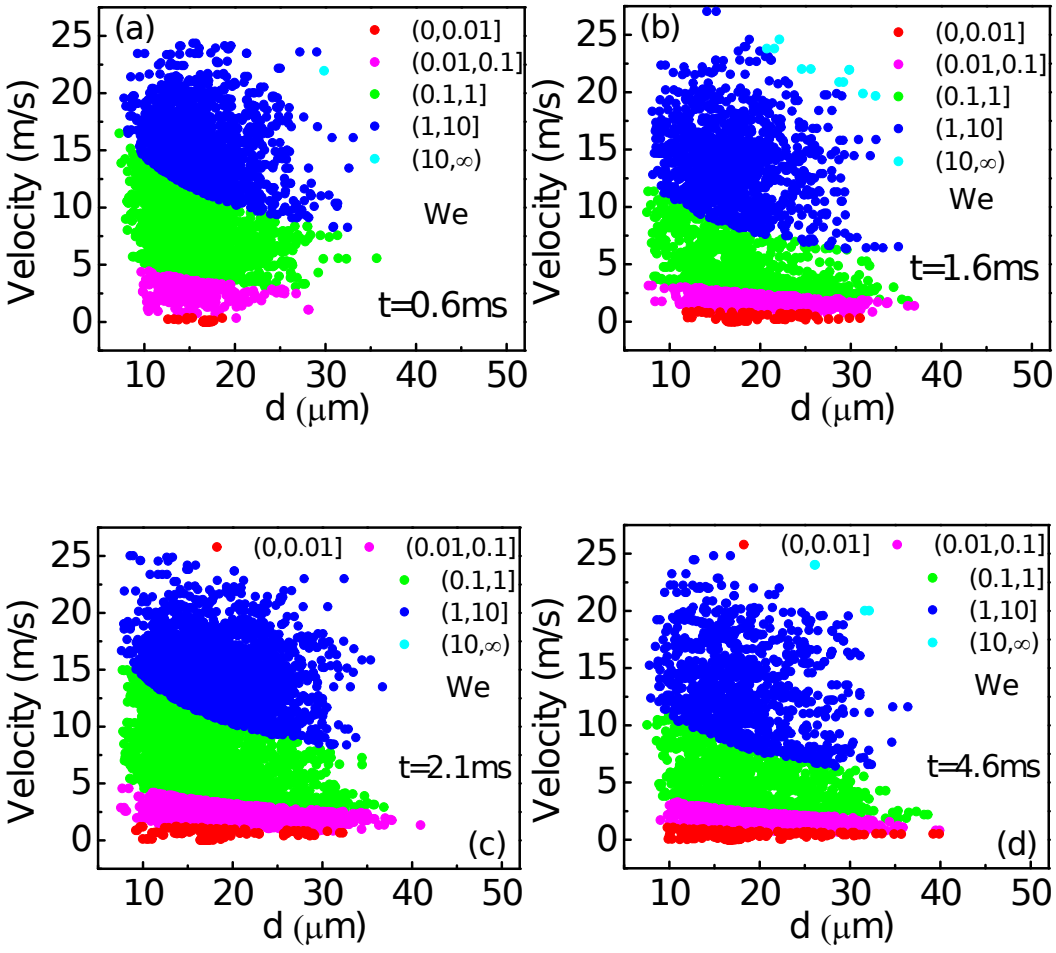

Figure 13 Range of *We* of all droplets during Stage II (t = 0.6 and 1.6 ms) and Stage III (t =2.1 and 4.6 ms)

The Weber numbers of each droplet at typical instants of t = 0.6, 1.6, 2.1 and 4.6 ms are presented in Figure 13. It is seen that the majority of the weber numbers is small and varies between 0.1 ~ 10. Some droplets have the Weber number smaller than 0.1, or even 0.01, but very few have the Weber number larger than 10.

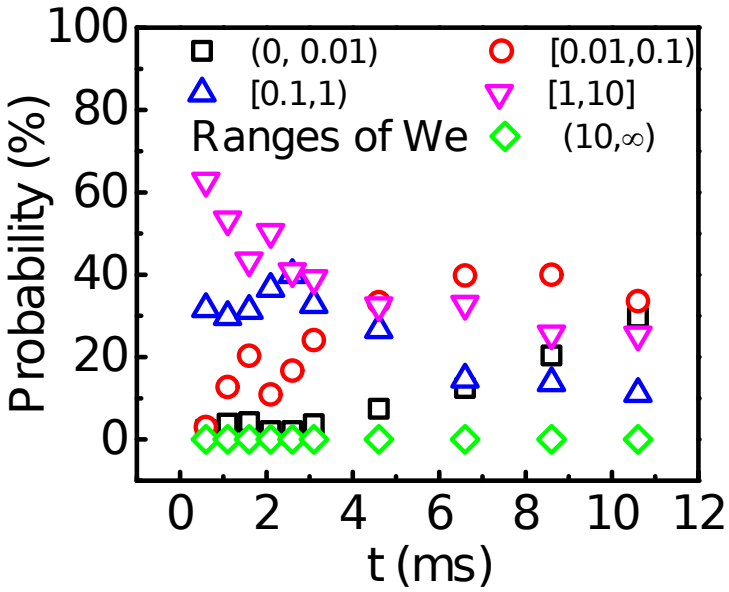

Figure 14 Variation of probabilities of droplet Weber numbers with time.

4. Conclusions

A set of measurements of droplet size and velocity in one dilute region of diesel spray were conducted by using the PDIA method. Evolution and statistics of droplet size and velocity were examined in a fixed location that is 40mm below the nozzle tip and 6 mm off the spray axis. Based on these data, PDFs about droplets were constructed.

Based on the experimental measurement, the whole unsteady process of spray development can be divided into three stages: the latency stage (0 - 0.5 ms), the injection stage (0.5 - 2.1 ms) and the free stage (after 2.1ms). In terms of droplet

statistics, the first stage is irrelevant because the spray tip has just arrived at the measurement location and no discrete droplets were detected.

In the second stage, both dense spray region and dilute spray region are observed and s plenty of discrete droplets are dispersed from the spray. The number probability of smaller droplets decreases with time and that of the bigger droplets increases, resulting in the increase of the total SMD. The velocity distribution presents an opposite trend. In addition, the seemingly disordered movement of the droplets shows a tendency to the outer side of the test window.

In the third stage, many droplet clouds are disappeared and the whole test window is filled with discrete droplets. The droplet density gradually decreases with time. The SMD decreases first because of the increase of the number of smaller droplets drifted from the inner side of the test window. After that, the SMD and the velocity reach an “equilibrium state”.

PDFs for droplet diameter were constructed and they can be well fitted in the form of lognormal function with nearly constant amplitude and standard variance. Through the analysis on droplet Stokes number and Weber number, it is concluded that the constructed PDFs reflect the characteristics of spray/droplets, and they are not strongly affected by the gaseous phase.

Acknowledgement

This work at Xi’an Jiaotong University was supported by the National Natural Science Foundation of China 51722603 and the Science Challenging Program (TZ201601). The work at the Hong Kong Polytechnic University was supported by the Hong Kong Research Grants Council/General Research Fund (PolyU 152217/14E and PolyU 152651/16E).

References

[1] K.D. Noritsune, Sakaguchi; Hironobu, Ueki; Masahiro, Ishida, Effect of injection pressure on droplet behavior inside diesel fuel sprays, SAE, 2015-01-1841 (2015).

[2] R. Payri, J.P. Viera, H. Wang, L.M. Malbec, Velocity field analysis of the high density, high pressure diesel spray, Int. J. Multiphase Flow, 80 (2016) 69-78.

[3] H. Hiroyasu, M. Arai, Structures of fuel sprays in diesel engines, SAE, 900475 (1990).
[4] S. Moon, Y. Matsumoto, K. Nishida, J. Gao, Gas entrainment characteristics of diesel spray injected by a group-hole nozzle, Fuel, 89 (2010) 3287-3299.
[5] X. Wang, Z. Huang, O.A. Kuti, W. Zhang, K. Nishida, Experimental and analytical study on biodiesel and diesel spray characteristics under ultra-high injection pressure, Int. J. Heat Fluid Flow, 31 (2010) 659-666.
[6] J. Tian, M. Zhao, W. Long, K. Nishida, T. Fujikawa, W. Zhang, Experimental study on spray characteristics under ultra-high injection pressure for DISI engines, Fuel, 186 (2016) 365-374.
[7] P. Rosin, E. Rammler, The laws governing the fineness of powdered coal, J. Inst. Fuel, 7 (1933) 29-36.
[8] S. Nukiyama, Y. Tanasawa, An experiment on the atomization of liquid. : 4th report, The effect of the properties of liquid on the size of drops, Trans. Jpn. Soc. Mech. Eng, 5 (1939) 131-135.
[9] F.A. Williams, Combust. Theory, 1985.
[10] R. Payri, B. Tormos, F.J. Salvador, L. Araneo, Spray droplet velocity characterization for convergent nozzles with three different diameters, Fuel, 87 (2008) 3176-3182.
[11] A. Urbán, M. Zaremba, M. Malý, V. Józsa, J. Jedelský, Droplet dynamics and size characterization of high-velocity airblast atomization, Int. J. Multiphase Flow, 95 (2017) 1-11.
[12] A.P. Kulkarni, D. Deshmukh, Spatial drop-sizing in airblast atomization-an experimental study, Atomization Sprays, 27 (2017) 949-961.
[13] J. Lee, K. Nishida, Breakup process of an initial spray injected by a D.I. gasoline injector-simulaneous measurement of droplet size and velocity by laser sheet image processing and partical tracking technique, SAE Tech. Pap. Ser., 2003-01-3107 (2003).
[14] K. Komada, D. Sakaguchi, H. Tajima, H. Ueki, M. Ishida, Relation between Tip Penetration and Droplet Size of Diesel Spray, SAE, 1 (2013).
[15] Y. Li, H. Guo, X. Ma, J. Wang, H. Xu, Droplet dynamics of DI spray from sub-atmospheric to elevated ambient pressure, Fuel, 179 (2016) 25-35.
[16] J. Jedelsky, M. Maly, N. Pinto del Corral, G. Wigley, L. Janackova, M. Jicha, Air–liquid interactions in a pressure-swirl spray, Int. J. Heat Mass Transfer, 121 (2018) 788-804.
[17] J.T. Kashdan, J.S. Shrimpton, A. Whybrew, Two-Phase Flow Characterization by Automated Digital Image Analysis. Part 2: Application of PDIA for Sizing Sprays, Part. Part. Syst. Charact., 21 (2004) 15-23.
[18] J.T. Kashdan, J.S. Shrimpton, A. Whybrew, A digital image analysis technique for quantitative characterisation of high-speed sprays, Optics and Lasers in Engineering, 45 (2007) 106-115.
[19] P. Keller, T. Knorsch, M. Wensing, C. Hasse, Experimental and numerical analysis of iso-octane/ethanol sprays under gasoline engine conditions, Int. J. Heat Mass Transfer, 84 (2015) 497-510.
[20] D. Jing, F. Zhang, Y. Li, H. Xu, S. Shuai, Experimental investigation on the macroscopic and microscopic spray characteristics of dieseline fuel, Fuel, 199 (2017) 478-487.
[21] R.S. Pathania, S.R. Chakravarthy, P.S. Mehta, Time-resolved characterization of low-pressure pulsed injector, Atomization Sprays, 26 (2016) 755-773.
[22] Z. Feng, C. Zhan, C. Tang, K. Yang, Z. Huang, Experimental investigation on spray and atomization characteristics of diesel/gasoline/ethanol blends in high pressure common rail injection system, Energy, 112 (2016) 549-561.

[23] L. Guan, C. Tang, K. Yang, J. Mo, Z. Huang, Effect of di-n-butyl ether blending with soybean-biodiesel on spray and atomization characteristics in a common-rail fuel injection system, Fuel, 140 (2015) 116-125.
[24] A.S. Jebakumar, J. Abraham, Comparison of the structure of computed and measured particle-laden jets for a wide range of Stokes numbers, Int. J. Heat Mass Transfer, 97 (2016) 779-786.
[25] C.B. Solnordal, C.Y. Wong, A. Zamberi, M. Jadid, Z. Johar, Determination of erosion rate characteristic for particles with size distributions in the low Stokes number range, Wear, 305 (2013) 205-215.
[26] A. Wierzba, DEFORMATION AND BREAKUP OF LIQUID-DROPS IN A GAS-STREAM AT NEARLY CRITICAL WEBER NUMBERS, Exp. Fluids, 9 (1990) 59-64.
[27] A.K. Flock, D.R. Guildenbecher, J. Chen, P.E. Sojka, H.J. Bauer, Experimental statistics of droplet trajectory and air flow during aerodynamic fragmentation of liquid drops, Int. J. Multiphase Flow, 47 (2012) 37-49.
[28] Z. Liu, R.D. Reitz, An analysis of the distortion and breakup mechanisms of high speed liquid drops, Int. J. Multiphase Flow, 23 (1997) 631-650.
[29] Product-Manual for DAVIS 8.0. 1003014_ParticleMaster_Shadow_D80.pdf, (2011).
[30] C. Baumgarten, Mixture Formation in Internal Combustion Engines, 110 (2006) A43.
[31] D.R. Guildenbecher, C. López-Rivera, P.E. Sojka, Secondary atomization, Exp. Fluids, 46 (2009) 371-402.